Geochimica et Cosmochimica Acta 420 (2026) 280–292

Contents lists available at ScienceDirect

Geochimica et Cosmochimica Acta

journal homepage: www.elsevier.com/locate/gca

Mineral transformations driven by *Acidimicrobium* sp. A6 increase the bioavailability of crystalline Fe oxides in co-cultures with *Geobacter sulfurreducens*

Jinhee Park [a], Joshua Atkinson [a,b], Shan Huang [a], Bruce E. Koel [c], Peter R. Jaffé [a,*]

[a] Department of Civil and Environmental Engineering, Princeton University, Princeton, NJ 08544, USA
[b] Omenn-Darling Bioengineering Institute, Princeton University, Princeton, NJ 08544, USA
[c] Department of Chemical and Biological Engineering, Princeton University, Princeton, NJ 08544, USA

ARTICLE INFO

Associate Editor: Juan Liu

Keywords:
Feammox
Acidimicrobium sp. A6
Geobacter
Goethite transformation
Microbial Fe(III) reduction
Iron cycling
Redox coupling
Ammonium oxidation

ABSTRACT

The bioavailability of Fe oxides critically governs microbial redox processes in natural and engineered systems. *Acidimicrobium* sp. A6 (A6), an autotrophic Feammox bacterium that oxidizes ammonium anaerobically coupled to Fe(III) reduction, has attracted interest for its potential relevance in the bioremediation of per- and polyfluoroalkyl substances (PFAS). However, its role in modulating Fe mineral transformations and interactions with other iron reducing bacteria under environmentally relevant conditions remains unclear. Here, we investigated Fe oxide transformations and microbial activity in A6, *Geobacter sulfurreducens*, and co-cultures of the two organisms amended with ferrihydrite or goethite across contrasting pH and nutrient conditions. Under acidic, oligotrophic conditions, Feammox activity was sustained while *G. sulfurreducens* was inhibited, demonstrating that selective A6 stimulation can be achieved through environmental control. Under circumneutral, nutrient-rich conditions, A6 and *G. sulfurreducens* coexisted, especially in goethite-amended systems. Fe K-edge X-ray absorption spectroscopy showed that A6 facilitated the transformation of crystalline goethite into less crystalline goethite, along with the emergence of Fe(II)-bearing phases, consistent with enhanced Fe(III) accessibility. Correspondingly, goethite-amended incubations supported sustained Feammox and stimulated acetate oxidation in co-cultures, highlighting the role of A6 in promoting Fe bioavailability for heterotrophic Fe(III) reducers. Together, these findings establish A6 as a robust Feammox performer and biological modulator of crystalline Fe oxides, supporting its potential for *in situ* applications in Fe(III)-rich environments.

1. Introduction

Crystalline Fe(III) oxides such as goethite (α-FeOOH) and hematite (α-Fe_2O_3) are thermodynamically stable and prevalent in weathered soils and sediments (Hansel et al., 2003; Roden and Urrutia, 2002; Zachara et al., 2002). Despite their environmental abundance, these oxides exhibit low microbial bioavailability due to limited solubility and slow reductive dissolution kinetics (Bonneville et al., 2009; Cutting et al., 2009; Hansel et al., 2005; Ravel and Newville, 2005; Zachara et al., 1998). In contrast, poorly crystalline ferrihydrite ($(Fe^{3+})_2O_3{\cdot}0.5H_2O$) is commonly used in laboratory studies of dissimilatory metal reduction due to its high surface area and reactivity (Hansel et al., 2005; Lovley and Phillips, 1988), although its metastability limits practical use in field applications (Hansel et al., 2003; Zachara et al., 2002).

Acidimicrobium sp. A6 (hereafter referred to as A6) is an autotrophic bacterium that couples anaerobic ammonium oxidation with the reduction of solid-phase Fe(III) (Huang and Jaffé, 2018), a process known as Feammox. In addition to its role in nitrogen and iron cycling, A6 has been shown to defluorinate persistent perfluoroalkyl substances (PFAS), such as perfluorooctanoic acid (PFOA) and perfluorooctanesulfonic acid (PFOS), during Feammox, highlighting its potential for integrated contaminant removal in anaerobic environments (Huang and Jaffé, 2019; Huang et al., 2022; Huang et al., 2024a; Park et al., 2023; Sima et al., 2023). However, most studies to date have been performed under highly selective, A6-favorable conditions—acidic pH and ferrihydrite amendments—where other dissimilatory iron-reducing bacteria (DIRB), such as *Geobacter* spp., are poorly

* Corresponding author.
E-mail address: jaffe@princeton.edu (P.R. Jaffé).

https://doi.org/10.1016/j.gca.2026.03.050
Received 21 November 2025; Accepted 28 March 2026
Available online 1 April 2026

competitive (Huang and Jaffé, 2018; Huang and Jaffé, 2019; Huang et al., 2022; Huang et al., 2024a; Huang et al., 2024b; Park et al., 2023; Ruiz-Urigüen et al., 2022).

In natural environments with circumneutral pH, *Geobacter* spp.—fast-growing heterotrophic DIRB with doubling times of hours to days (Bond and Lovley, 2003; Huang and Jaffé, 2018)—may outcompete A6 for electron acceptors. Because these organisms can thrive across a broad pH range (5.5–7.0) (Straub and Buchholz-Cleven, 2001; Wang et al., 2021; Xu et al., 2019), Fe(III) oxide amendments may inadvertently stimulate *Geobacter* spp., thereby reducing Fe(III) availability for A6. Thus, understanding the competitive dynamics between A6 and *Geobacter* spp. under different Fe(III) mineral regimes is essential for optimizing A6-driven bioremediation strategies.

Solid-phase Fe(III) delivery remains a logistical constraint in subsurface systems due to mineral aggregation and sediment sorption (Jaffé et al., 2024). Although our prior work demonstrated that polyacrylic acid (PAA)-coated ferrihydrite enhances Feammox activity by improving colloidal stability and electron transfer (Park et al., 2023), the instability of ferrihydrite under environmental conditions still poses a barrier to long-term application. In contrast, crystalline oxides such as goethite and hematite are more geochemically persistent and commercially available, yet their bioavailability to A6—and potential for use in field-scale systems—remains poorly understood.

In this study, we evaluated the bioavailability of ferrihydrite and goethite for A6 and *G. sulfurreducens* under pure and co-culture conditions across a range of pH and media. We further assessed whether A6 could enhance the accessibility of crystalline Fe oxides by modifying their mineral structure. Structural changes in Fe speciation and crystallinity were characterized using X-ray diffraction (XRD) and Fe K-edge X-ray absorption spectroscopy (XAS) with linear combination fitting (LCF). To assess whether A6 can remain functionally active and modulate Fe oxide bioavailability in the presence of other heterotrophs under less selective, more environmentally relevant conditions, we also conducted incubations using A6-enrichment cultures containing diverse microbial communities. These experiments were performed under co-culture optimized conditions (near neutral pH, nutrient-rich media), with or without *G. sulfurreducens*, to evaluate the broader applicability of A6-mediated Feammox and mineral transformation.

By integrating microbial activity measurements with mineralogical analyses, this work provides mechanistic insights into the role of A6 in modulating Fe oxide bioavailability. These findings inform strategies to selectively stimulate A6 in complex microbial environments and advance anaerobic bioremediation processes in Fe(III)-rich systems dominated by crystalline Fe oxides.

2. Materials and methods

2.1. Preparation of Fe oxides

Two-line ferrihydrite ($(Fe^{3+})_2O_3{\cdot}0.5H_2O$) was synthesized following a modified procedure described by Schwertmann and Cornell (2008). In brief, an aqueous solution of iron(III) nitrate nonahydrate ($Fe(NO_3)_3{\cdot}9H_2O$, ≥ 98%, Sigma-Aldrich, USA) was titrated with 1 M KOH to adjust the pH to between 7 and 8. The resulting suspension was dialyzed until the pH stabilized, then rinsed twice with deionized water, and stored at 4 °C until use. Prior to culture incubation, ferrihydrite suspensions were further rinsed with deionized water by centrifugation and handled under ambient temperature and pressure conditions. Crystalline Fe oxides, including goethite (α-FeOOH, powder, 30–63% Fe; Sigma-Aldrich, Cat. No. 71063) and hematite (α-Fe_2O_3, powder, ≥ 99.8% purity; STREM Chemicals, Cat. No. 93–2617) were obtained commercially.

In addition to commercial goethite, a less crystalline goethite was synthesized following the method of Nakamura et al. (2013). Specifically, 160 mL of 0.1 M $FeCl_3$ solution was mixed with 40 mL of 2.5 M NaOH and incubated at 60 °C for 24 h. The resulting yellow-orange suspension was cooled to room temperature, dialyzed using a cellulose tubular membrane until the pH stabilized at 8.8, rinsed with deionized water, harvested by centrifugation, and dried. This material is hereafter referred to as "less crystalline goethite" to distinguish it from the more crystalline, commercially available goethite used in this study.

2.2. Characterization of Fe samples

The surface morphology of ferrihydrite, hematite, and goethite was examined using environmental scanning electron microscopy (ESEM) under high-vacuum conditions at 10 kV with a working distance of 9.7–10.1 mm. To assess Fe mineral transformations during microbial incubations, X-ray diffraction (XRD) and Fe K-edge X-ray absorption near-edge structure (XANES) spectroscopy were performed.

Fe K-edge XANES spectra were acquired to determine Fe oxidation states and mineralogical composition. Linear combination fitting (LCF) was conducted using representative reference minerals commonly found in natural environments, including ferrihydrite ($(Fe^{3+})_2O_3{\cdot}0.5H_2O$), crystalline goethite (α-FeOOH), less crystalline goethite, lepidocrocite (γ-FeO(OH)), magnetite (Fe_3O_4), and siderite ($FeCO_3$). Detailed instrumental settings, spectral processing, and LCF procedures are described in the Supporting Information (SI) (Text S1). The LCF fitting results for all samples and the underlying spectral data are available in a Zenodo repository (https://doi.org/10.5281/zenodo.17672259).

To evaluate the crystallinity and solubility of Fe oxides used in culture incubations, we performed chemical extraction using 3 M HCl for 24 h followed by Fe quantification via the ferrozine assay (Stookey, 1970). Because the ferrozine assay quantifies Fe(II), Fe(III) released during acid extraction was subsequently reduced to Fe(II) using hydroxylamine hydrochloride prior to analysis (Viollier et al., 2000). Accordingly, the measured Fe concentrations represent the total acid-extractable Fe (reported as Fe(II)), rather than native Fe(II). These values are used as a comparative indicator to distinguish poorly crystalline (*i.e.,* labile phases) from highly crystalline Fe oxides based on their acid solubility.

2.3. Incubations of A6 pure culture under A6-favored conditions

Acidimicrobium sp. A6 was incubated under autotrophic conditions optimized for Feammox activity (pH 4.5) and no added organic carbon source (Park et al., 2023) in a defined medium (Sawayama, 2006). The per-liter medium composition was: 0.2 g NH_4Cl, 0.04 g $(NH_4)_2SO_4$, 0.02 g $NaHCO_3$, 0.07 g $KHCO_3$, 0.01 g K_2HPO_4, 0.05 g $MgSO_4{\cdot}7H_2O$, and 0.06 g $CaCl_2$. 1 mL of vitamin solution (ATCC MD-VS), 1 mL of trace element solution (Amer and Kim, 2023). To promote extracellular electron transfer, 25 μM anthraquinone-2,6-disulfonate (AQDS) was added (Huang and Jaffé, 2018). Cultures were amended with ferrihydrite, hematite, or goethite (5 mM Fe) as the sole electron acceptor.

All incubations were conducted in biological triplicates in serum bottles sealed with butyl rubber stoppers and aluminum crimps. Anaerobic conditions were achieved by evacuating headspace and purging with an N_2/CO_2 gas mixture (80:20, v/v). Cultures were prepared in 60 mL serum bottles by inoculating a 10-fold dilution of A6 stock culture into the prepared medium. Cultures were incubated at 25 °C in the dark on a rotary shaker for 68 days. Autoclaved controls (121 °C, 20 min) were included for the goethite-amended conditions to confirm biological Fe reduction and ammonium oxidation. A6 activity was assessed by monitoring ammonium removal over time and quantifying 16S rRNA gene copy numbers using quantitative PCR (qPCR). Genomic DNA was extracted with the DNeasy PowerSoil Pro Kit (Qiagen), and amplification was performed on a StepOnePlus™ Real-Time PCR System (Thermo Fisher Scientific) using primers *acm_v1F/acm_v1R* (5′-GGCGGCGTGCTTAACACAT-3′ / 5′-GAGCCCGTCCCA-GAGTGATA-3′), as described by Ruiz-Urigüen et al. (Ruiz-Urigüen et al., 2022). Reactions (20 μL) contained 10 μL SYBR® Premix Ex Taq™ II, 0.8 μL of each primer (10 nM), 0.4 μL ROX reference dye, 6 μL DI

water, and 2 μL DNA template. The thermal cycling protocol included 94 °C for 30 s (initial denaturation), followed by 40 cycles of 94 °C for 5 s, 57 °C for 30 s, and 70 °C for 30 s. Each sample was run in technical triplicates with no-template controls. Standard curves were generated using plasmids containing cloned A6 16S rRNA gene fragments. Only reactions with amplification efficiencies between 90 and 110% and R^2 values above 0.98 were considered valid.

2.4. Incubations of G. sulfurreducens pure cultures under Geobacter-favored conditions

Geobacter sulfurreducens PCA (ATCC 51573) was used as a model dissimilatory Fe(III)-reducing bacterium. Precultures were grown to mid-log phase in *Geobacter* growth medium (Marsili et al., 2008) containing (per liter): 0.38 g KCl, 0.2 g NH_4Cl, 0.069 g $NaH_2PO_4{\cdot}H_2O$, 0.04 g $CaCl_2{\cdot}2H_2O$, and 0.2 g $MgSO_4{\cdot}7H_2O$ (Marsili et al., 2008), following pH adjusted to 6.5, 2.0 g $NaHCO_3$, 10 mL trace mineral solution, 10 mL vitamin solution (ATCC MD-VS) (Chan et al., 2015; Lovley and Phillips, 1988) and amended with 10 mM acetate and 40 mM fumarate as electron donor and acceptor, respectively. Cells were harvested by centrifugation (4920 × g for 20 min), washed twice with sterile 30 mM sodium bicarbonate buffer (pH 7.1) (Coppi et al., 2001), and resuspended in fresh *Geobacter* growth medium to the desired cell density.

Experimental incubations were conducted using *Geobacter* growth medium amended with ferrihydrite or goethite (5 mM as Fe) as the sole electron acceptor, with 10 mM acetate as the electron donor. AQDS (25 μM) was added to all cultures to maintain consistency with A6 incubations. Anaerobic conditions were established by purging with an 80:20 N_2/CO_2 gas mixture and sealing with butyl rubber stoppers and aluminum crimps. All cultures were incubated at 25 °C in the dark on the rotary shaker for 21 days in biological triplicates.

Geobacter activity was monitored by measuring acetate concentrations and quantifying 16S rRNA gene copy numbers via qPCR using the primer pair 561F/825R (Stults et al., 2001) (5′-GCGTGTAGGCGGTTTCTTAA-3′/5′-TACCCGCRACACCTAGTTCT-3′). qPCR run details were identical to those used for A6.

2.5. Co-culture experimental design

To assess the influence of A6 on *G. sulfurreducens* activity, incubations were performed with ferrihydrite or goethite, using two growth media (A6 growth medium or *Geobacter* growth medium), and each at a pH of 4.5 and 6.5. *G. sulfurreducens* pure cultures were incubated with ferrihydrite under all pH–medium combinations and with goethite only in *Geobacter* medium. A6 pure cultures were incubated with ferrihydrite under all conditions and with goethite only in A6 medium. Co-cultures were established with ferrihydrite or goethite across all pH–medium combinations.

All cultures were inoculated with laboratory-maintained stocks into the designated growth conditions. A6 and *G. sulfurreducens* were inoculated at initial densities of approximately 10^4 and 10^6 16S rRNA gene copies mL^{-1}, respectively. Sodium acetate (10 mM) was supplied to *G. sulfurreducens* pure cultures and co-cultures but omitted from A6 pure cultures. Ferrihydrite or goethite (10 mM as Fe) was provided as the sole electron acceptor. While reactive surface area is a critical factor influencing reaction kinetics, the total Fe(III) dose was maintained constant across all treatments to ensure a consistent electron acceptor pool. This approach was prioritized given the high stoichiometric demand for Fe (III) in the studied biological processes: Feammox (6 mol Fe reduced per mol ammonium oxidized) and acetate oxidation by *G. sulfurreducens* (8 mol Fe reduced per mol acetate oxidized). Consequently, the molar concentration of Fe(III) serves as a primary constraint on sustained biological activity and overall redox cycling in these systems. Anaerobic incubations were conducted in biological triplicates at 25 °C in the dark for 50 days. Autoclaved controls (121 °C for 20 min) were included for each Fe oxide–pH–medium combination to confirm the absence of microbial activity. To avoid thermal- or pressure-induced mineral alterations, synthesized ferrihydrite was prepared separately, rinsed three times with deionized water, centrifuged after each rinse, and then added aseptically to the autoclaved media. This differentiated approach was employed to maintain the mineralogical integrity of the less stable Fe phases throughout the incubation. Culture conditions were monitored over time by measuring ammonium, acetate, Fe(II), pH, and redox potential (Eh). Detailed sampling and analytical protocols are provided in Text S2.

2.6. Incubations of A6 enrichment cultures and co-cultures with G. sulfurreducens under environmentally relevant conditions (pH 6.5, Geobacter medium)

To evaluate the bioavailability of ferrihydrite and goethite for A6 under environmentally relevant conditions, A6 enrichment cultures (containing a diverse microbial community but excluding *G. sulfurreducens*), *G. sulfurreducens* pure cultures, and co-cultures were incubated with either ferrihydrite or goethite (20 mM as Fe) in *Geobacter* medium at pH 6.5. The A6 enrichment culture used in this study was originally derived from sediment collected at the Assunpink Wildlife Management Area (NJ, USA), as described by Huang and Jaffé (2015). Since its establishment, the culture has been maintained under strictly anaerobic conditions at room temperature (20–25 °C) and routinely transferred (~every six months) into fresh Feammox medium to sustain Feammox activity and community stability. The enrichment has been regularly monitored for community composition, A6 abundance, and Feammox activity to ensure long-term consistency in metabolic performance.

A higher Fe concentration (20 mM) was employed in this experiment—compared to the 5 and 10 mM used in previous incubations—to prevent potential Fe limitation, particularly in co-cultures containing a broader microbial community. However, the elevated Fe concentration posed challenges for DNA extraction and qPCR quantification of A6.

A6 enrichment cultures were prepared by inoculating a tenfold dilution of active A6 cultures into suspensions containing autoclaved *G. sulfurreducens* cells. Conversely, *G. sulfurreducens* pure cultures were prepared by diluting active *G. sulfurreducens* cells into suspensions containing autoclaved A6 cultures. Co-cultures were established by co-inoculating active A6 and *G. sulfurreducens* cultures at initial densities of approximately 10^4 and 10^6 16S rRNA gene copies mL^{-1}, respectively. These ratios were chosen to reflect the relative abundance of A6 to *Geobacter* spp. (0.01–0.13) typically observed in constructed wetland mesocosms (Shuai and Jaffé, 2019). This approach ensured comparable starting concentrations of acetate and ammonium across all treatments.

Anaerobic incubations followed previously described methods (Huang and Jaffé, 2015) and cultures were incubated at 25 °C in the dark for 26 days. Microbial activity was assessed by monitoring ammonium, acetate, Fe(II) concentrations, and Eh over time, and mineralogical changes were evaluated by XRD and XANES–LCF for Fe solids, as described in Text S2.

2.7. Statistical analyses

Time-dependent differences within each treatment were assessed using paired t-tests or one-way repeated-measures ANOVA with Bonferroni-adjusted pairwise comparisons. Comparisons between independent treatments at the same sampling time were analyzed using two-tailed independent t-tests. Statistical significance was determined at $p < 0.05$.

3. Results and discussion

3.1. A6-driven Feammox activity with different Fe oxides under A6-favored conditions

To assess A6-driven Feammox activity as a function of Fe oxide type, A6 cultures were incubated with ferrihydrite (FH), hematite (HM), or goethite (GT). These oxides span a range of crystallinity—from poorly crystalline ferrihydrite to highly crystalline goethite and hematite—and are commonly found in soils and sediments at pH > 4 (Lentini et al., 2012).

Prior to incubation, each Fe oxide was characterized for morphology, crystallinity, and solubility (Fig. S1). ESEM revealed distinct morphologies, while 3 M HCl extraction followed by ferrozine quantification indicated varying solubility and labile Fe content. As expected, ferrihydrite was nearly fully dissolved, whereas hematite and goethite released less extractable Fe, with goethite showing the lowest solubility, confirming its designation as the most crystalline Fe oxide (Fig. S1D). Additionally, commercial and synthesized goethite was included as a reference mineral for XANES analysis (Fig. S2). Although their overall solubility was extremely low, the synthesized goethite released moderately more extractable Fe than the commercial goethite. This observed increase in reactivity, along with its broader and less intense XRD peaks (Fig. S2A), and the distinct features in the post-edge region of the Fe K-edge spectra (Fig. S2B and C), provides a consistent basis for our terminology. Accordingly, synthesized goethite is referred to as "less crystalline goethite" in this study.

A6 cultures were grown in A6 growth medium with ferrihydrite, hematite, or goethite. Ammonium was monitored as a proxy for Feammox activity (Fig. 1A). All treatments exhibited significant ammonium removal by day 24 ($p < 0.05$), with no substantial changes thereafter. Despite differences in Fe oxide crystallinity, ammonium removal remained comparable across treatments.

A6 growth was confirmed by 16S rRNA gene quantification (Fig. 1B). A6 abundance increased to similar extents across all Fe oxide treatments, demonstrating its ability to grow with both poorly and highly crystalline Fe oxides. Together, these results indicate that A6-mediated Feammox activity was not strongly influenced by Fe oxide crystallinity under the tested conditions.

Notably, soluble Fe(II) accumulation was modest (Fig. S3A). This pattern likely reflects the limited decrease in redox potential in the autotrophic A6 cultures, which may have prevented the stable persistence of Fe(II) in the soluble phase. Even if Fe(III) was partially reduced, the resulting Fe(II) may have been rapidly reoxidized by nitrite (Jaffé et al., 2024) and/or reincorporated into Fe(III) oxides via surface electron transfer (Sheng et al., 2020), thereby obscuring the net Fe(II) accumulation despite the ongoing Feammox activity.

To further probe Fe mineral transformations, total labile Fe was tracked via 3 M HCl extraction followed by hydroxylamine reduction (Fig. S3B). Extractable Fe decreased across all treatments by day 24, with pronounced declines observed in the goethite- and hematite-amended samples. This trend suggests that part of the Fe pool was altered by microbial activity but did not manifest as soluble or extractable Fe(II). Instead, Fe(II) may have been reincorporated into less labile secondary phases or retained within more crystalline matrices that resist dissolution by HCl. Overall, the decrease in extractable Fe(III) provides indirect evidence of A6-mediated mineral transformations in crystalline oxide systems, despite limited Fe(II) accumulation.

To gain structural insights beyond solubility-based data, Fe K-edge XANES was conducted on goethite-amended samples collected at day 0 and day 68. Linear combination fitting (LCF) indicated that the initial Fe phase was dominated by crystalline goethite (Fig. 1C), consistent with the fact that goethite was the only Fe oxide supplied to the incubations. Thus, the overwhelming proportion of crystalline goethite detected at day 0 can be attributed to the experimentally added mineral, while only a minor fraction of other Fe phases may have originated from the A6 inoculum. By day 68, however, the solid-phase Fe assemblage shifted, with the emergence of less crystalline goethite accompanied by Fe(II)-bearing phases such as siderite, indicating partial microbial reduction of Fe(III) by A6. Prior studies have shown that dissimilatory Fe (III)-reducing bacteria (DIRB) can induce localized structural modifications or defect generation in crystalline Fe oxides without disrupting bulk crystallinity (Cutting et al., 2009). Although the specific mechanism of Fe reduction by A6 remains unclear, the observed mineralogical shifts suggest that A6 can partially transform crystalline goethite, potentially enhancing its bioavailability during extended incubations.

Taken together, despite limited Fe(II) accumulation, the combined evidence of ammonium removal, A6 growth, decreases in extractable Fe, and XANES-based mineralogical changes strongly supports A6-mediated Feammox activity across all Fe oxide treatments. These findings demonstrate that A6 can oxidize ammonium using Fe(III) oxides of varying crystallinity as terminal electron acceptors under acidic conditions.

3.2. G. sulfurreducens activity with different Fe oxides under Geobacter-favored conditions

To assess the bioavailability of crystalline Fe oxides to a model DIRB, *Geobacter sulfurreducens* cultures were incubated with either ferrihydrite or goethite at pH 6.8 in *Geobacter* growth medium. These conditions were selected to reflect optimal growth and Fe(III) reduction. *G. sulfurreducens* was inoculated at a lower density (10^4 copies/mL; Fig. 2B) compared to the A6 cultures (10^6 copies/mL; Fig. 1B). This low inoculation accounted for the much faster doubling time of

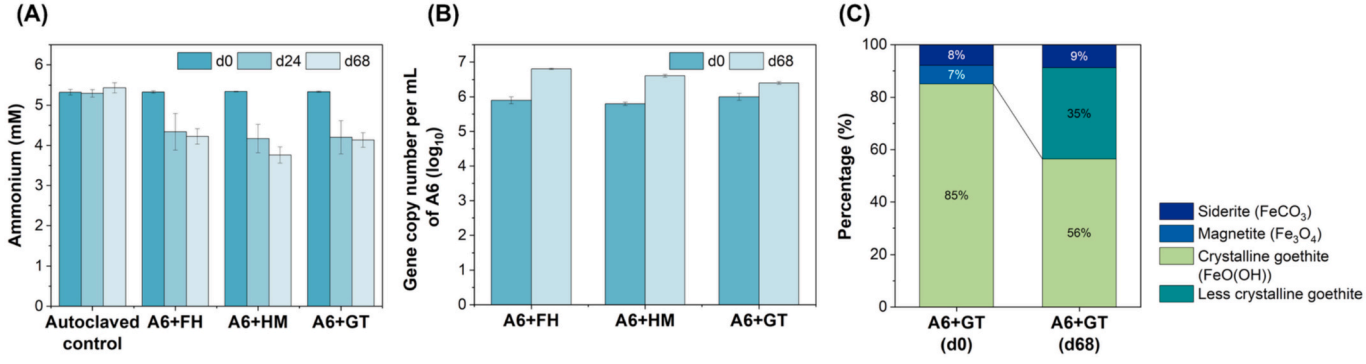

Fig. 1. (A) Ammonium concentrations in A6 cultures incubated with ferrihydrite (FH), hematite (HM), or goethite (GT) at pH 4.5 for 68 days. "Autoclaved control" indicates a sterilized GT control. Error bars show mean ± SD (n = 3). (B) 16S rRNA gene copy numbers of A6 before and after incubation (log_{10} copies/mL). (C) Fe mineral composition in A6 + GT samples before and after incubation, determined by linear combination fitting (LCF) of Fe K-edge XANES spectra. The goodness of fit for pre- and post-incubation samples was indicated by the R factor (2.62×10^{-4} and 8.39×10^{-5}) and reduced χ^2 values (6.43×10^{-5} and 7.55×10^{-2}).

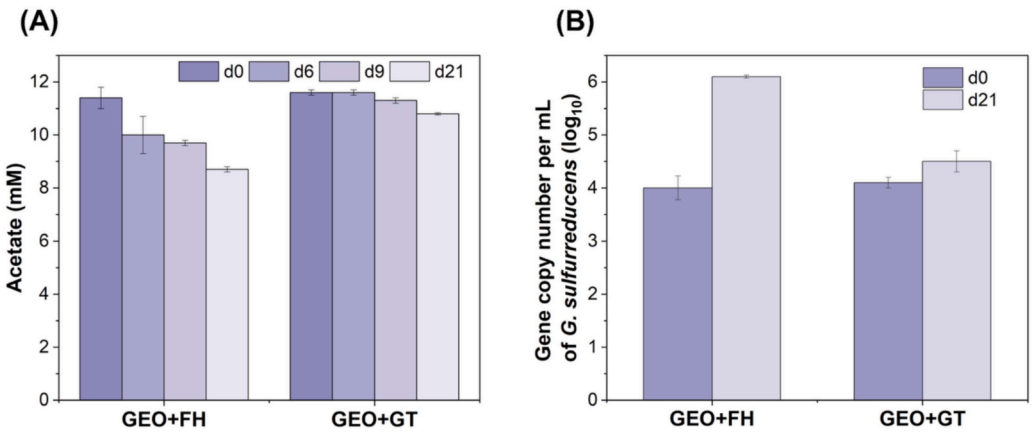

Fig. 2. (A) Acetate concentrations in *G. sulfurreducens* (GEO) cultures incubated with FH or GT. (B) 16S rRNA gene copy numbers of *G. sulfurreducens* in GEO cultures before (d0) and after incubation (d21). Data represent the mean ± SD of biological replicates (n = 3).

G. sulfurreducens relative to A6. Accordingly, *G. sulfurreducens* cultures were incubated for 21 days, shorter than the 68-day period used for A6, ensuring a comparable growth window across both organisms and minimizing the risk of early substrate depletion or Fe(III) reduction saturation.

The influence of Fe oxide type on *G. sulfurreducens* activity was evaluated by monitoring acetate concentrations over time (Fig. 2A). In ferrihydrite-amended cultures, acetate was steadily consumed throughout the incubation period, reflecting the high bioavailability of ferrihydrite. In contrast, goethite-amended cultures exhibited minimal acetate removal until after day 6 ($p > 0.05$), followed by a gradual decline with statistically significant differences thereafter ($p < 0.05$). This result is consistent with previous findings that crystalline goethite is less bioavailable than ferrihydrite for *G. sulfurreducens* (Notini et al., 2019).

16S rRNA gene quantification corroborated these trends, showing higher *G. sulfurreducens* abundance in ferrihydrite-amended cultures than in goethite-amended cultures at the end of incubation (Fig. 2B). Overall, the greater acetate consumption and higher *G. sulfurreducens* abundance in ferrihydrite treatments indicates that ferrihydrite remained more bioavailable than goethite to *G. sulfurreducens* under *Geobacter*-favored conditions.

3.3. pH and medium composition shape A6-Geobacter interactions in pure and co-cultures

A6-mediated bioremediation may benefit from selectively stimulating A6 while limiting competition from other DIRB, such as *Geobacter* spp., especially when Fe oxide availability is limited. Results from the previous sections showed that A6-driven ammonium oxidation occurred independent of Fe oxide type under A6-favored conditions (Fig. 1A), whereas *G. sulfurreducens*-mediated acetate oxidation was significantly enhanced when amorphous ferrihydrite was used as the electron acceptor (Fig. 2A). These findings indicate that the choice of Fe oxide could be leveraged to selectively stimulate A6 activity in the presence of *G. sulfurreducens*.

To further examine how Fe oxide type influences interactions between A6 and *G. sulfurreducens*, we incubated pure and co-cultures with ferrihydrite or goethite for 50 days under different combinations of pH (4.5 or 6.5) and growth media (A6Med or GeMed) (Fig. 3A). A6Med represents an oligotrophic medium, while GeMed contains higher concentrations of phosphate, bicarbonate, minerals, and vitamins. The selected pH values reflect either acidic conditions favorable to A6 or a circumneutral pH (6.5) that supports growth of both A6 and *G. sulfurreducens*. For pure cultures, each organism was incubated with both ferrihydrite or goethite in its respective optimal medium, while cross-incubations in the medium of the other organism were conducted only with ferrihydrite due to its higher bioavailability. Co-cultures were incubated with both Fe oxides across all combinations of pH and media (Fig. 3A).

We evaluated the activity of A6 and *G. sulfurreducens* in both pure and co-cultures at both pHs. *G. sulfurreducens* activity was monitored by measuring acetate, while A6 activity was monitored by measuring ammonium. As shown in Figs. 3B–E, acetate concentrations remained stable at pH 4.5 but declined significantly ($p < 0.05$) at pH 6.5 across all treatments. This confirms that *G. sulfurreducens* activity is strongly pH-dependent and suppressed under acidic conditions. In contrast, ammonium removal by A6 occurred at both pH 4.5 and 6.5 (Figs. 3F–I), indicating that A6 remains active under both low and circumneutral pH. These results show that acidic conditions can selectively suppress *G. sulfurreducens* while still supporting A6-driven Feammox.

Medium composition also influenced microbial activity. In *G. sulfurreducens* cultures with ferrihydrite, acetate removal reached 26.1% in GeMed compared to 19.8% in A6Med (Fig. 3C). Correspondingly, Fe(II) concentrations reached 5.8 mM in GeMed by day 6, versus 5.9 mM in A6Med only by day 25 (Fig. S4A), suggesting faster *Geobacter*-mediated Fe(III) reduction in GeMed. In A6 cultures, ammonium removal on day 26 showed no significant differences between A6Med and GeMed at either pH (Figs. 3F and G). However, in co-cultures, more pronounced ammonium depletion occurred in GeMed, particularly at pH 6.5 (Figs. 3H and I). This enhancement may be attributed to nutrient components in GeMed that favor A6 activity, with additional contributions potentially from ammonium assimilation by *G. sulfurreducens*. Consistent with this interpretation, *G. sulfurreducens* pure cultures exhibited a negligible ammonium change at pH 4.5 but a significant decrease at pH 6.5 ($p < 0.05$; Fig. S5), indicating assimilation-driven nitrogen uptake under growth-permissive conditions. Accordingly, ammonium removal in co-cultures reflects the combined contributions from the A6-mediated Feammox activity and ammonium assimilation by *G. sulfurreducens*. Notably, even when ammonium decreases observed in the *G. sulfurreducens* pure cultures are taken as a conservative upper bound for assimilation, the co-cultures still showed a substantially greater ammonium depletion, indicating a sustained A6-associated activity under these conditions.

Together, these observations highlight the role of nutrient composition in modulating both microbial activity and interspecies interactions: Nutrient limitations in A6Med restrict *G. sulfurreducens* while remaining permissive for A6 activity, whereas GeMed at pH 6.5 supports both organisms, leading to more dynamic microbial interactions. Thus, in addition to pH, nutrient limitations in A6Med likely restrict *G. sulfurreducens* activity, presenting a strategy to promote A6 while minimizing competition for Fe oxides. Conversely, under favorable

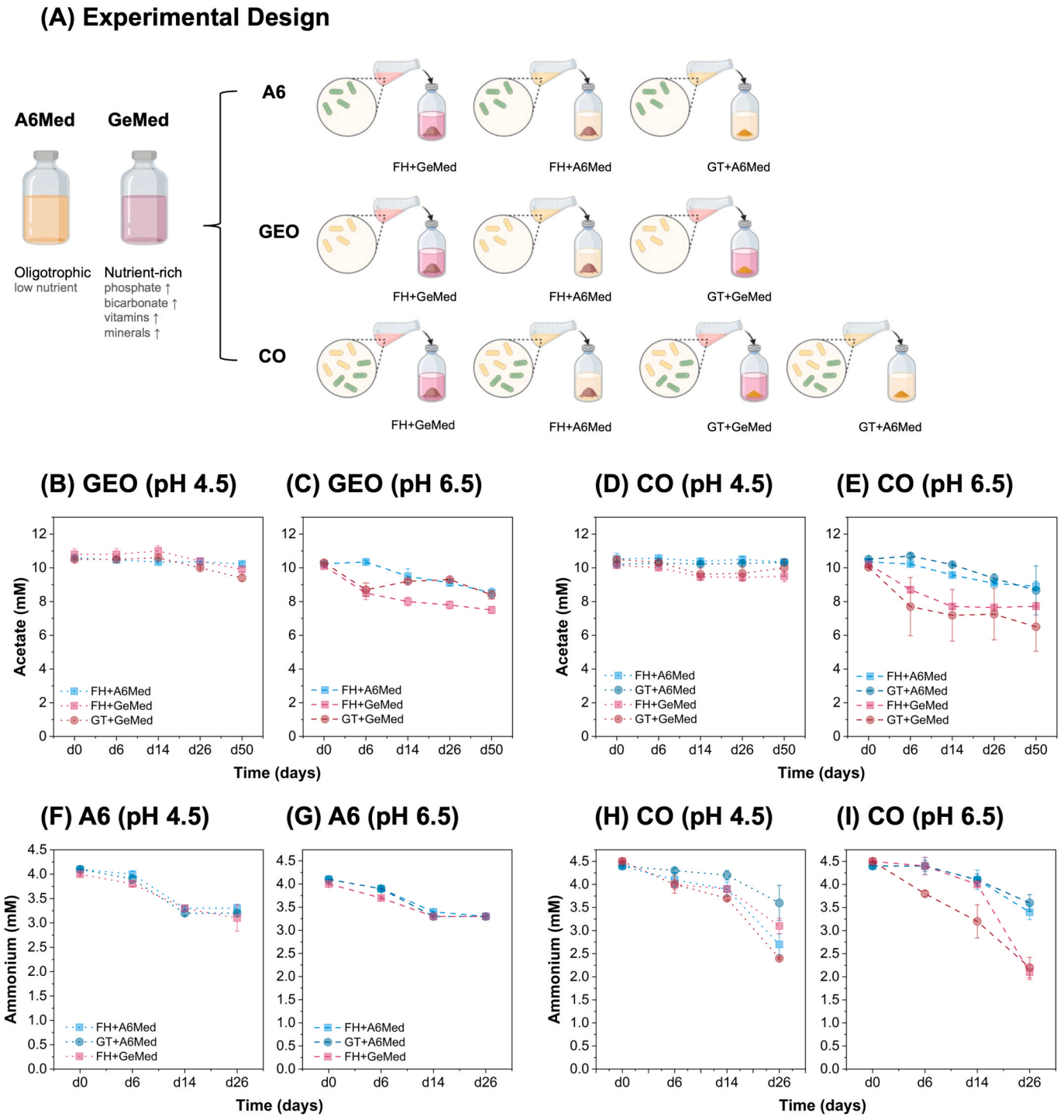

Fig. 3. Experimental design and temporal changes in acetate and ammonium concentrations in A6 (A6), *G. sulfurreducens* (GEO), and co-culture (CO) incubations with ferrihydrite (FH) or goethite (GT) under varying pH and medium conditions. (A) Schematic of the experimental setup. Illustration created with BioRender under a publication license. (B–E) Temporal profiles of acetate in GEO and CO cultures: (B) GEO at pH 4.5, (C) GEO at pH 6.5, (D) CO at pH 4.5, and (E) CO at pH 6.5. (F–I) Temporal profiles of ammonium in A6 and CO cultures under corresponding conditions: (F) A6 at pH 4.5, (G) A6 at pH 6.5, (H) CO at pH 4.5, and (I) CO at pH 6.5. Data represent mean ± SD (n = 3).

conditions for both organisms (pH 6.5 with GeMed), more dynamic microbial interactions must be considered.

3.4. Fe oxide type modulates bioavailability and microbial redox activity under co-culture favorable conditions

To isolate the influence of the Fe oxide type under conditions favorable to both organisms, we compared ferrihydrite- and goethite-amended co-cultures incubated at pH 6.5 in GeMed. We begin by examining ferrihydrite incubations, where acetate oxidation in co-cultures closely resembled that in *G. sulfurreducens* pure cultures, indicating that A6 did not inhibit *G. sulfurreducens* activity (Figs. 3C and E). Final acetate concentrations were not significantly different between pure and co-cultures ($p > 0.05$), and negligible acetate loss was observed in autoclaved controls (Fig. S6). However, in ferrihydrite-amended co-cultures, ammonium concentrations declined more steeply than in A6

cultures, especially in GeMed (Figs. 3G and I), suggesting enhanced Fe (III) reduction driven by A6 or assimilation by *G. sulfurreducens*. Consistently higher Fe(II) concentrations in co-cultures (Fig. S4B) further corroborate this enhanced activity.

Despite enhanced Fe(II) production in co-cultures, Fe(II) concentrations remained far below than the theoretical maximum expected from the complete oxidation of both acetate and ammonium (Table S1). Electron recovery analysis revealed that only 42–45% of electrons derived from acetate and ammonium were recovered as extractable Fe (II) in the co-cultures. This yield was slightly higher than that of *G. sulfurreducens* pure cultures (22–31%), suggesting additional Fe(III) reduction via A6-mediated Feammox.

A portion of the unrecovered electrons may have been diverted toward biomass synthesis, particularly by *G. sulfurreducens*. Previous studies have shown that a variable fraction of acetate-derived electrons, depending on growth conditions and the electron acceptor, can be allocated to cell growth (Esteve-Núñez et al., 2005). For example, under fumarate-respiring conditions, approximately 23.6% of the electrons were directed to biomass, whereas only 6.5% were used when soluble $FeCl_3$ served as the electron acceptor. Given that our experiments used solid-phase Fe(III) (ferrihydrite), which is generally less bioavailable than $FeCl_3$, it is plausible that a larger fraction of electrons was required for cell maintenance or stress adaptation, further reducing Fe(II) recovery in our system.

In addition, Fe(II) accumulation may have been underestimated due to its abiotic reoxidation by nitrite—a byproduct of Feammox—or precipitation as poorly soluble secondary Fe minerals such as lepidocrocite and magnetite, which can form during biologically mediated Fe(III) reduction (Boland et al., 2014; Hansel et al., 2005; Nevin and Lovley, 2002). Notably, Fe(II) concentrations declined after day 25 (Fig. S4), suggesting that a portion of Fe(II) became non-extractable in 3 M HCl due to mineral transformations. These findings emphasize the importance of providing excess Fe(III) in future co-culture incubations to prevent electron acceptor limitation and to enable more accurate quantification of Fe(III) reduction under co-metabolic conditions.

Redox measurements further supported the interpretation that Fe(II) accumulation was suppressed by abiotic nitrite reoxidation and mineral precipitation. At pH 6.5, Eh decreased by 288 mV in *G. sulfurreducens* cultures and 232 mV in co-cultures (Figs. S7B and D), reflecting distinct redox trajectories in the presence versus absence of A6. In contrast, at pH 4.5, the final bulk Eh values (d50) were higher than the initial values (d0) across all treatments (Figs. S7A and C). This can be attributed to the strong suppression of *G. sulfurreducens* activity, as evidenced by the lack of measurable acetate consumption (Fig. 3). Under these conditions, especially in the co-cultures, although A6-driven Feammox occurred, localized and transient Fe(II) production was insufficient to induce a net decrease in bulk Eh, as such Fe(II) was likely consumed by the aforementioned abiotic or localized redox processes. In the absence of sustained acetate oxidation to provide continuous reducing power, the system-wide redox balance shifted, and the bulk Eh consequently drifted toward higher values over time. pH dynamics offered additional mechanistic insights. In ferrihydrite-amended treatments, pH increased over time—reaching ~7.0 in *G. sulfurreducens* cultures and 7.2 (GeMed) or 6.9 (A6Med) in co-cultures (Figs. S8B and D). This likely reflects OH^- generation during acetate oxidation, and H^+ consumption during Feammox. However, since Feammox is thermodynamically less favorable above pH 7, the observed pH increase may have contributed to declining A6 activity in the later stages. Together, these findings indicate that ferrihydrite supports concurrent metabolic activity by A6 and *G. sulfurreducens* under circumneutral, nutrient-rich conditions.

Distinct trends emerged in the goethite-amended incubations depending on the presence of A6. Under conditions favorable to both organisms (pH 6.5, GeMed), co-cultures exhibited a higher average acetate removal than the *G. sulfurreducens* pure cultures, resulting in lower final acetate concentrations (Figs. 3C and E). This contrasts with the ferrihydrite-amended incubations, where acetate oxidation was comparable between the pure and co-cultures, consistent with an intrinsically higher bioavailability of ferrihydrite. Under these conditions, the absence of measurable enhancement in co-cultures further suggests that A6 did not directly stimulate *G. sulfurreducens* activity. In contrast, in goethite-amended systems, although *G. sulfurreducens* alone was capable of reducing and utilizing goethite under these conditions, the greater acetate depletion observed in co-cultures suggests that the presence of A6 may have increased the effective bioavailability of goethite. Increased acetate oxidation in these co-cultures likely supported greater *G. sulfurreducens* growth, which could in turn increase ammonium assimilation under growth-permissive conditions. However, as discussed above, even when ammonium decreases observed in *G. sulfurreducens* pure cultures are considered as a conservative reference for assimilation-driven uptake, the magnitude and pattern of ammonium loss in goethite-amended co-cultures remain consistent with concurrent A6-associated ammonium oxidation. Accordingly, ammonium concentrations declined more steeply in the goethite-amended co-cultures than in other tested conditions (Fig. 3I), further supporting active nitrogen turnover under these conditions. Despite evidence of enhanced Fe reduction, only low levels of Fe(II) were detected in all goethite-amended co-cultures (Fig. S4B). As with A6 cultures, this likely reflects the low solubility of goethite, abiotic reoxidation of Fe(II) by intermediates such as nitrite, or the formation of poorly soluble secondary Fe minerals. These processes may have limited the detectable aqueous Fe(II), despite active microbial Fe(III) reduction. Eh and pH dynamics further support these interpretations. Final pH values reached 7.0 (GeMed) and 6.7 (A6Med) (Fig. S8D), indicating robust microbial metabolism. Correspondingly, Eh declined substantially—to 70 mV in GeMed and –36 mV in A6Med (Fig. S7D). These redox shifts are consistent with *Geobacter*-mediated acetate oxidation and may be facilitated by A6-induced enhancement of goethite bioavailability, rather than competitive inhibition, as A6 does not utilize acetate. Importantly, A6 did not suppress *Geobacter* activity under any tested condition. Instead, increased acetate oxidation and clear ammonium depletion in goethite-amended co-cultures contrast with the trends observed in ferrihydrite-amended incubations, where both organisms exhibited comparable activity levels.

3.5. A6 modulates Fe oxide bioavailability in a diverse microbial community under environmentally relevant conditions

To evaluate whether Fe oxide type influences A6-driven processes in a more complex microbial community, we incubated a mixed enrichment culture containing A6 but lacking *G. sulfurreducens* (A6-mix), *G. sulfurreducens* pure cultures (GEO), and co-cultures of A6-mix amended with *G. sulfurreducens* (CO) under environmentally relevant conditions (pH 6.5, GeMed). Each culture was amended with either ferrihydrite or goethite. Acetate was omitted from A6-mix cultures to suppress heterotrophic activity, thereby isolating ammonium oxidation primarily attributable to Feammox. Following 26 days of the incubation, ammonium concentration decreased by ~20–23% in A6-mix cultures amended with either ferrihydrite or goethite, with no significant differences between treatments except for a transient effect at day 14 ($p = 0.04$) (Fig. 4A). These results suggest that A6-mediated ammonium oxidation was not strongly constrained by Fe oxide crystallinity in A6-mix cultures, consistent with observations in A6 cultures (Fig. 1A). Notably, in these A6-mix cultures, no appreciable decrease in Eh or accumulation of HCl-extractable Fe(II) was observed (Figs. 4C and E). This lack of measurable Fe(II) was attributed to the absence of acetate, which precluded a substantial drop in redox potential typically driven by heterotrophic organic carbon oxidation. Under these conditions, any Fe(II) generated via Feammox likely remained in a transient state, being rapidly reoxidized by reaction intermediates (e.g., nitrite) or immobilized within the mineral lattice. This decoupling of net Fe(II) concentrations from the extent of ammonium oxidation precluded the establishment of a formal stoichiometric mass balance for the A6-

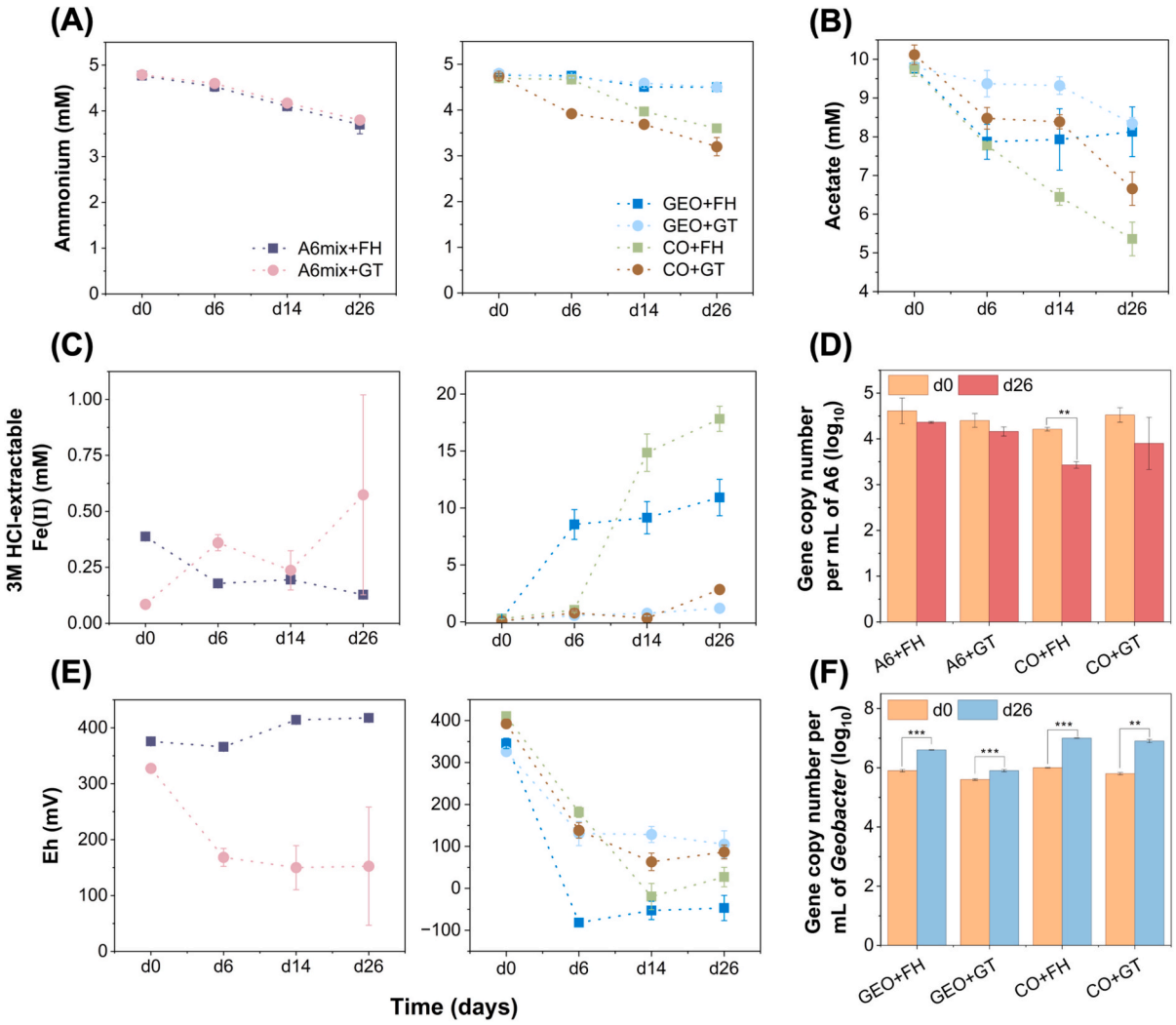

Fig. 4. Microbially mediated reactions under environmentally relevant conditions (pH 6.5, GeMed). Data represent mean ± SD (n = 3). Panels (A), (C), and (E) each contain two subpanels: the left subpanel shows A6-enrichment cultures (A6mix), and the right subpanel shows *G. sulfurreducens* pure cultures (GEO) and co-cultures (CO). Time-dependent changes in (A) ammonium, (B) acetate, (C) 3 M HCl-extractable Fe(II), and (E) redox potential (Eh) are shown for A6-enrichment cultures (A6-mix), *G. sulfurreducens* (GEO), and co-cultures (CO) amended with ferrihydrite (FH) or goethite (GT) over 26 days. A6-mix cultures were incubated without acetate, whereas GEO and CO cultures were supplied with acetate as a carbon source and electron donor. Panels (D) and (F) show 16S rRNA gene copy numbers (log_{10} scale) of A6 and *G. sulfurreducens*, respectively, measured at day 0 and day 26. Asterisks indicate statistically significant differences between day 0 and day 26 within the same treatment (*$p < 0.05$, **$p < 0.01$, ***$p < 0.001$).

enrichment systems, a phenomenon that will be further substantiated by mineralogical evidence in Section 3.6.

Ammonium removal in co-cultures with *G. sulfurreducens*, driven by a combination of A6-mediated Feammox and heterotrophic assimilation, was comparable to or greater than in A6-mix cultures alone—achieving 23% and 32% removal in ferrihydrite- and goethite-amended systems, respectively (Fig. 4A). In contrast, *G. sulfurreducens* cultures showed minimal ammonium loss (< 6%), likely reflecting assimilation for biomass synthesis. To estimate the potential contribution of heterotrophic assimilation to ammonium removal in co-cultures, we applied a correction based on literature-reported biomass yields for *G. sulfurreducens* grown under contrasting electron-acceptor conditions. Specifically, carbon conversion efficiencies of 6.5% ($FeCl_3$-grown culture) and 23.6% (fumarate-grown cultures), together with a representative C:N ratio of 6.58 derived from fumarate-grown cultures (Esteve-Núñez et al., 2005; Howley et al., 2022), were used to define a plausible range of assimilation-driven ammonium uptake. Because A6-mix cultures include additional heterotrophic community members beyond *G. sulfurreducens*, assimilation by the broader microbial community cannot be fully constrained using this correction. Accordingly, the adjustment was applied to reduce potential overestimation of Feammox-driven ammonium oxidation in co-cultures and to facilitate comparison of Fe oxide–dependent trends, rather than to achieve strict stoichiometric closure.

$$\begin{aligned} &Corrected\,A6-driven\,ammonium\,oxidation\,(mM) \\ &= \Delta[ammonium]_{co-cultures} - (\Delta[acetate] \times 2 \times yield\,coefficient \div C:N\,ratio) \end{aligned} \quad (1)$$

Corrected values revealed distinct trends depending on Fe oxide type (Fig. S9). In ferrihydrite-amended incubations, A6-driven ammonium oxidation was consistently higher in A6-mix cultures than in co-cultures, suggesting a competitive suppression by faster-growing DIRB. In contrast, goethite-amended co-cultures showed greater A6-mediated ammonium oxidation than A6-mix cultures, indicating that A6 more effectively accessed goethite under less competitive conditions.

Acetate removal occurred in all treatments but was slower in goethite-amended *G. sulfurreducens* cultures (Fig. 4B), reflecting the limited bioavailability of goethite for *G. sulfurreducens*. In ferrihydrite-

amended systems, acetate depletion initially proceeded at similar rates in pure and co-cultures but diverged after day 14, with co-cultures showing enhanced removal—likely due to synergistic activity between *G. sulfurreducens* and other heterotrophs. Consistent with this explanation, Fe(II) accumulation in the co-cultures exceeded that in the pure cultures after day 14 (Fig. 4C), reflecting a concurrent Fe(III) reduction processes in the co-cultures, including contributions from both *G. sulfurreducens* and A6.

Interestingly, co-cultures exhibited redox dynamics that appeared to delay early Fe(II) accumulation. By day 6, HCl-extractable Fe(II) was substantially higher in *G. sulfurreducens* pure cultures than in co-cultures (Fig. 4C), despite comparable acetate removal. This discrepancy coincided with contrasting Eh values: –82 mV in pure cultures vs +182 mV in co-cultures (Fig. 4E). These observations are consistent with the dynamics described in Section 3.4, where Feammox activity coupled with Fe(II) reoxidation (e.g., by nitrite) likely suppressed net Fe(II) accumulation. As incubation progressed, Eh in co-cultures declined, reaching –20 mV by day 14, and Fe(II) accumulation increased accordingly—reflecting ongoing A6-driven Feammox alongside heterotrophic Fe (III) reduction.

Goethite-amended co-cultures consistently exhibited greater acetate removal than *G. sulfurreducens* pure cultures (Fig. 4B). Due to the low HCl solubility of goethite, Fe(II) accumulation could not be reliably quantified as in ferrihydrite systems. Nevertheless, a small Fe(II) increase was detected in co-cultures by day 26 (Fig. 4C), suggesting limited release of labile Fe(II), possibly via A6-mediated Feammox—consistent with enhanced ammonium oxidation in these cultures. Both goethite-amended treatments also showed steady Eh declines (Fig. 4E), confirming that oxidation of organic carbon generated reducing conditions. However, Eh values in goethite systems consistently remained higher than those in ferrihydrite systems, indicating that goethite buffers redox shifts more effectively under reducing conditions.

The 16S rRNA gene copy number of *G. sulfurreducens* increased by approximately one order of magnitude across all treatments after 26 days of incubation, with higher levels observed in co-cultures (Fig. 4F). This trend corresponded with enhanced acetate oxidation and Fe(II) accumulation relative to the pure cultures. Among the treatments, goethite-amended pure cultures exhibited the smallest increase, whereas both ferrihydrite- and goethite-amended co-cultures showed comparable *G. sulfurreducens* abundance, indicating that the presence of A6 did not inhibit its growth.

In contrast, the 16S rRNA gene copy number of A6 did not increase in any treatment after 26 days, which is not surprising, given its slow doubling time ~10 days (Fig. 4D). A6 abundance remained within the same order of magnitude in both A6-mix cultures amended with either ferrihydrite or goethite, although goethite-amended incubations exhibited lower Eh values, indicating more reducing conditions (Fig. 4E). In co-cultures, where active acetate oxidation occurred through a more diverse microbial community, A6 16S rRNA gene copy numbers showed a modest decrease by day 26. Despite more reducing bulk Eh values in goethite-amended incubations (Fig. 4E), the A6 population growth was not enhanced. This observation is consistent with previous mesocosm studies showing that A6 abundance in the surface layer—where Eh remained relatively high (~400 mV) even after four months of operation—was comparable to, or only slightly lower than, that in deeper and more reducing layers (Shuai and Jaffé, 2019). Likewise, Feammox activity has been reported across a wide range of Eh values (e.g., 62.7–484.3 mV) (Li et al., 2015), suggesting that bulk Eh may not accurately represent the microscale redox conditions governing A6-mediated Feammox. Therefore, even though A6 abundance did not increase under the tested conditions, the levels observed in both A6-mix and co-cultures were likely sufficient to sustain Feammox activity. This interpretation agrees with prior findings that the extent of ammonium removal does not strongly correlate with A6 abundance, which has been attributed to limitations in electron-transfer sites on Fe oxide surfaces (Sima et al., 2023). Furthermore, as discussed above, the absence of a strict stoichiometric correlation between ammonium removal and Fe(II) accumulation does not negate Feammox activity; rather, it reflects the rapid internal cycling of Fe in these acetate-free systems. While bulk geochemical measurements alone cannot resolve these transient processes, the occurrence of A6-mediated Feammox is further substantiated by the mineralogical transformations detailed in Section 3.6. Consequently, these integrated findings provide robust evidence of sustained A6 metabolic activity despite the absence of substantial biomass increases.

While the present study does not resolve the mechanistic links among bulk redox potential, organic carbon availability, and A6 growth, our results demonstrate that ammonium oxidation and the associated Fe redox transformations persisted even in the absence of detectable A6 population growth. This finding suggests that the A6-associated metabolic activity can be maintained without substantial biomass accumulation under the tested conditions. However, the specific microscale processes governing Fe reduction, redox cycling, and microbial interactions cannot be directly resolved from bulk geochemical measurements alone, motivating further examination of Fe mineral transformations to better constrain how A6 influences Fe bioavailability. Taken together, these findings demonstrate that Fe oxide type strongly modulates redox dynamics and microbial access to electron acceptors in mixed communities. While A6 did not inhibit acetate oxidation by *G. sulfurreducens*, A6-driven ferrihydrite reduction appeared constrained by competition with faster-growing DIRB. In contrast, the lower bioavailability of goethite limited reduction by other microbes, providing A6 with a niche to perform Feammox under reduced competition. Through this mechanism, A6 may act as a modulator of Fe oxide bioavailability—altering goethite through partial reduction, redox cycling, or the release of mineral-associated organic matter. These changes can subsequently promote Fe reduction by heterotrophs, as suggested by late-stage Fe(II) buildup and enhanced acetate oxidation in co-cultures. In the following section, we examine mineralogical transformations to further clarify how A6 reshapes Fe availability and redox reactivity in diverse microbial systems.

3.6. Mineralogical transformations of Fe oxides in A6-enrichment co-cultures with G. sulfurreducens

To evaluate whether A6-mediated metabolism alters Fe mineral speciation and crystallinity, solid-phase Fe minerals from ferrihydrite- and goethite-amended incubations were analyzed at day 26 using XRD, Fe K-edge XANES with LCF, and ESEM (Figs. 5 and 6). In ferrihydrite-amended A6-mix cultures, XRD patterns retained the broad features of amorphous ferrihydrite with no detectable crystalline transformation products (Fig. 5A). In contrast, XANES–LCF revealed the presence of secondary Fe(II)-bearing minerals, including siderite and magnetite (Fig. 5C), indicating that Fe(III) reduction had occurred despite the absence of XRD-detectable phase changes. Nevertheless, extractable Fe (II) did not accumulate and bulk Eh remained relatively stable over the incubation period (Figs. 4C and E). This discrepancy likely reflects the transient nature of Fe(II) under Feammox conditions, where Fe(II) produced during ammonium oxidation can be rapidly reoxidized, for example by nitrite generated during Feammox or through surface-coupled electron transfer processes (Jaffé et al., 2024; Sheng et al., 2020). Together, these findings indicate that A6 reduced ferrihydrite, but secondary reactions masked net accumulation of soluble Fe(II).

In ferrihydrite-amended incubations of both *G. sulfurreducens* pure cultures (GEO) and co-cultures with A6-mix cultures (CO), XRD patterns revealed the formation of lepidocrocite as a secondary crystalline phase (Fig. 5A), which was also identified as a major component by XANES-LCF (Fig. 5C). In *G. sulfurreducens* pure cultures, the appearance of lepidocrocite coincided with stagnation of acetate oxidation and Fe(II) accumulation after day 14 (Figs. 4B and C), consistent with the lower microbial bioavailability of lepidocrocite relative to ferrihydrite

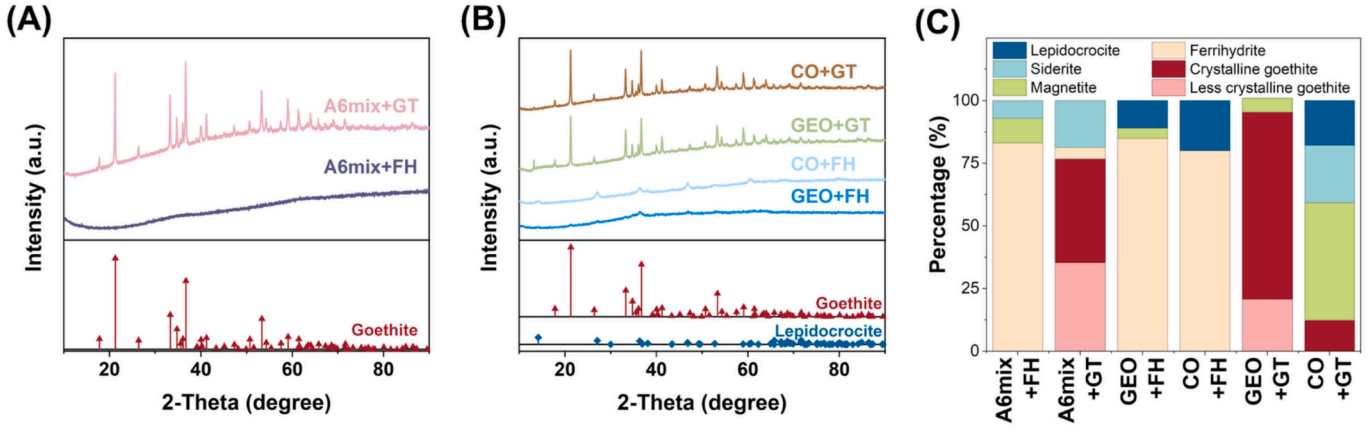

Fig. 5. Mineralogical changes in Fe composition at the end of incubation. (A–B) X-ray diffraction (XRD) patterns of (A) A6mix, (B) GEO, and CO cultures. Reference peaks for detected mineral phases are shown at the bottom. (C) Fe mineral composition (%) determined by Fe K-edge XANES–LCF, showing greater phase diversity than observed by XRD. Ferrihydrite or goethite was supplied at the start of incubation, and the compositions represent end-point Fe phases formed under each condition.

(O'loughlin et al., 2021). In contrast, co-cultures showed more pronounced lepidocrocite XRD peaks, suggesting increased crystallinity, yet Fe(II) continued to accumulate after day 14 (Fig. 4C). This observation implies that the presence of A6 sustained Fe(III) reduction even after transformation of ferrihydrite to less bioavailable crystalline phases, potentially through Feammox-driven Fe cycling.

In goethite-amended A6-mix cultures, XRD patterns showed negligible changes compared to pristine goethite (Fig. 5B), indicating that bulk crystallinity remained largely unchanged. However, XANES–LCF detected the formation of less crystalline goethite, ferrihydrite, and siderite (Fig. 5C and Table S2), suggesting that A6 activity altered goethite crystallinity and promoted the formation of secondary Fe phases at a scale not resolvable by XRD. Complementing these findings, ESEM imaging of the A6-mix cultures (Figs. 6A and B) revealed localized surface alterations, including the rounding of goethite rod ends and the presence of irregular, non-rod morphologies. The latter likely represents secondary precipitates formed through the reaction between transiently released Fe(II) and Feammox-derived intermediates (e.g., nitrite), providing direct visual evidence of A6-induced mineral restructuring even without extensive bulk transformation. Notably, redox potential showed a sustained decline over the incubation period (Fig. 4E), indicating the establishment of more reducing conditions conducive to Fe(II) persistence. Although acetate was not added to the A6-mix cultures, TOC analyses revealed that the commercial goethite contained measurable amounts of tightly bound organic carbon (~0.067 mg C g^{-1}), which was extractable only under acidic conditions. This observation suggests that structural modification of goethite by A6 may have mobilized mineral-associated organic matter (OM) that was otherwise inaccessible to microbes. The released OM may have further supported the growth of heterotrophic IRB, consistent with the microbial community shifts discussed in Text S3.

In goethite-amended *G. sulfurreducens* pure cultures, XRD patterns similarly showed no detectable bulk phase changes over the 26-day incubation (Fig. 5B), whereas XANES–LCF indicated the formation of less crystalline goethite and magnetite (Fig. 5C). In support of these observations, ESEM images (Fig. 6D) revealed secondary mineral morphologies, such as tabular and aggregated features, that differ from the pristine needle-like goethite. While these features may represent minor mineral phases that were not dominant enough to be resolved in the XANES–LCF, their presence provides critical evidence of localized Fe redistribution and mineral transformation not captured by XRD. Compared to *G. sulfurreducens* pure cultures, co-cultures exhibited a broader suite of secondary minerals, including lepidocrocite, siderite, and magnetite, together with diverse mineral morphologies observed by ESEM (Figs. 6E and F). This expanded mineral assemblage indicates that initially recalcitrant goethite underwent more extensive transformations when A6 and *G. sulfurreducens* coexisted. We propose a conceptual model in which A6 enhances the bioavailability of crystalline goethite primarily through localized surface modification and defect generation, while reductive dissolution likely occurs as a concomitant process (Fig. 7). Surface defects—such as under-coordinated surface Fe sites or Fe vacancies (Callister and Rethwisch, 2020)—have been shown to render goethite highly susceptible to preferential reduction (Notini et al., 2018; Notini et al., 2019). This localized surface reactivity is evidenced by the scoured and rounded rod ends observed in the A6-enrichment and *G. sulfurreducens* cultures (Figs. 6A and C), which are consistent with previous reports of preferential reduction at goethite rod ends (Cutting et al., 2009; Notini et al., 2019). Accordingly, the detection of "less crystalline goethite" by XANES–LCF likely reflects the development of these surface defects and the incorporation of Fe into structurally imperfect domains, rather than a significant bulk phase transformation.

Surface-associated Fe(II) produced during reduction may subsequently undergo Fe(II)–goethite interfacial electron transfer (Amstaetter et al., 2010; Latta et al., 2012), a process known to occur more readily at defect-rich sites and localized structural transformation (e.g., Fe(II)-catalyzed recrystallization) at goethite interfaces (Notini et al., 2018; Notini et al., 2019). While the absence of lattice-scale imaging, such as transmission electron microscopy (TEM), limits direct observation of individual defects, the integrated analysis of ESEM morphology, XANES coordination, Fe(II) accumulation, and Eh profiles provide a robust basis for this proposed mechanism of localized mineral restructuring.

In A6-enrichment cultures, HCl-extractable Fe(II) accumulation remained limited (Fig. 4C); however, the presence of secondary minerals—evidenced by amorphous morphologies in ESEM (Fig. 6B) and identified via XANES–LCF (Fig. 5C)—indicates that localized Fe release and reprecipitation processes occurred. Any Fe(II) transiently released into solution was likely rapidly reoxidized (e.g., via reaction with nitrite produced during Feammox) and subsequently precipitated as labile Fe (III) phases or secondary minerals. In co-cultures, A6 is thought to facilitate this transformation by initiating localized surface modifications that can increase the accessibility of goethite to *G. sulfurreducens*. Once these reactive sites are available, the subsequent Fe(III) reduction by *G. sulfurreducens* leads to a rapid increase in Fe(II) and more reducing conditions (Figs. 4C and E), which appears to promote extensive iron redistribution. This synergy, sustained by the continuous oxidation of ammonium and acetate, provides the thermodynamic driving force to maintain the Fe redox cycling and the diverse suite of secondary

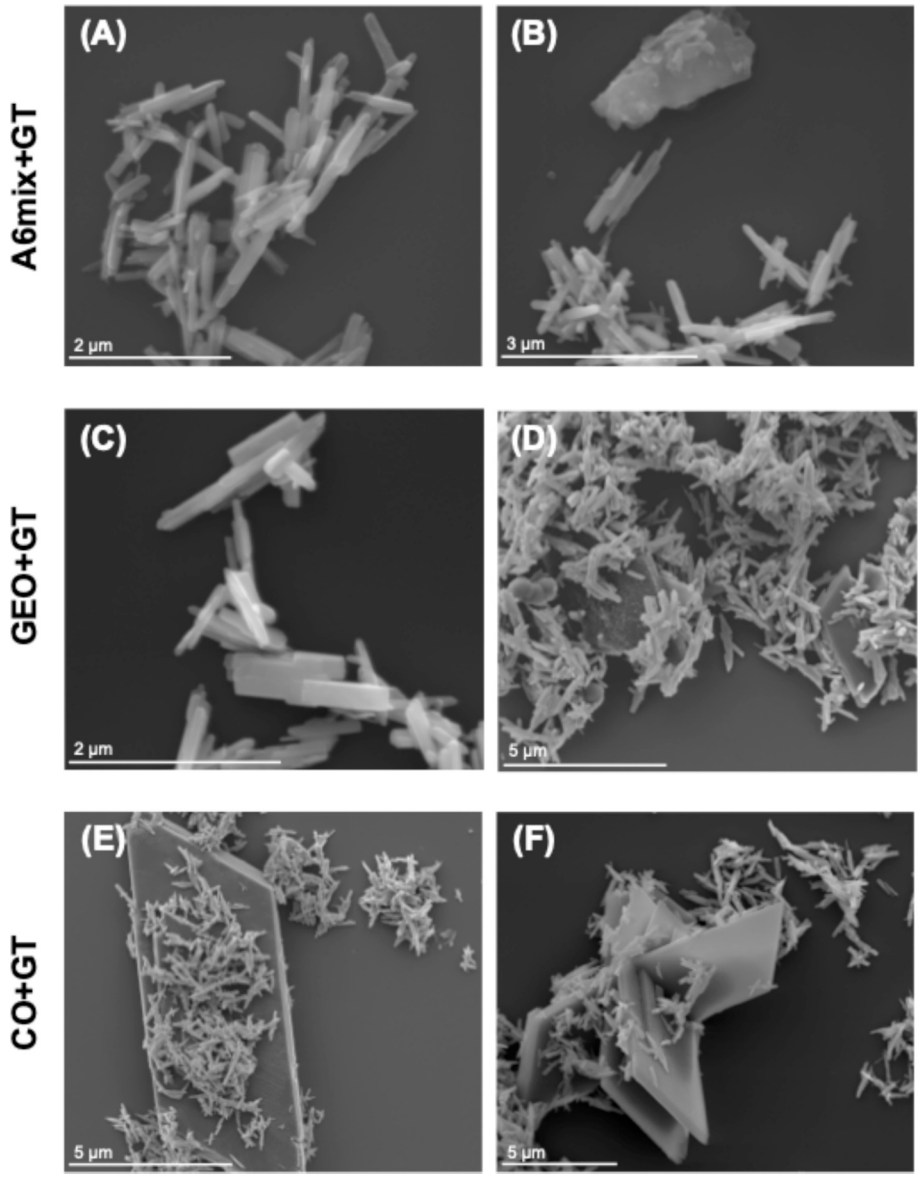

Fig. 6. Environmental scanning electron microscopy (ESEM) micrographs of goethite-amended incubations on day 26. (A–B) A6mix cultures showing localized scouring and rounding of goethite rod ends and the presence of irregular, non-rod morphologies (top). (C–D) GEO cultures exhibiting similar morphological alterations and secondary phase formation. (E–F) CO cultures displaying extensive mineral transformation, characterized by the development of diverse secondary mineral morphologies alongside remnants of goethite.

minerals most extensively observed in the co-culture systems. Overall, these results indicate that A6 not only reduces Fe(III) via Feammox but also modifies the structural characteristics of Fe oxides—particularly goethite—in ways that enhance their bioavailability to other DIRB in the environment. This dual role is especially important under environmentally relevant conditions where crystalline Fe oxides dominate, and bioavailable Fe is otherwise limited.

4. Conclusion

This study demonstrates that *Acidimicrobium* sp. A6 modulates the bioavailability of crystalline Fe oxides through Feammox activity, even under environmentally relevant conditions. While acidic, oligotrophic settings can suppress competing Fe reducers such as *G. sulfurreducens* and selectively favor A6, our findings reveal that A6 remains metabolically active and functionally significant in circumneutral, carbon-amended environments representative of field conditions. A6-driven Feammox partially reduced and restructured goethite, increasing Fe (III) accessibility for both A6 and coexisting dissimilatory Fe reducers. These mineralogical changes sustained ammonium and acetate oxidation and extended redox cycling, thereby broadening the ecological niche for Fe-dependent microbial processes. Because crystalline goethite is inexpensive, widely available, and less susceptible to microbial competition, especially under more acidic conditions, it may serve as an effective Fe source to stimulate A6-driven Feammox *in situ*. Future studies should assess the robustness of A6 under fluctuating redox conditions and stronger microbial competition to evaluate its field-scale potential. Additionally, while our multi-scale analysis provides strong evidence for mineralogical alterations, future investigations utilizing high-resolution imaging, such as TEM, will be instrumental in resolving the lattice-scale structural defects and crystallinity changes initiated by A6.

CRediT authorship contribution statement

Jinhee Park: Writing – original draft, Writing – review & editing,

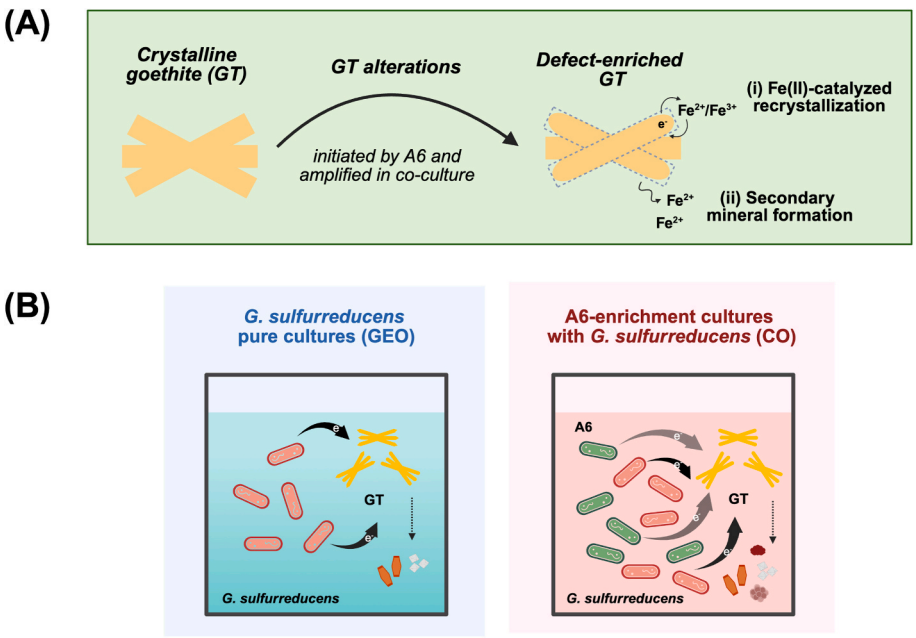

Fig. 7. (A) Schematic representation of the proposed mineral-scale processes occurring at the goethite surface, including localized surface modification (e.g., defect generation), Fe(II)-catalyzed interfacial electron transfer and recrystallization, and secondary mineral formation. (B) Conceptual depiction of goethite reduction dynamics in GEO and in CO cultures, highlighting differences in effective Fe bioavailability and mineral transformation. Illustration created with BioRender.com under a publication license.

Visualization, Validation, Methodology, Investigation, Formal analysis, Data curation, Conceptualization. **Joshua Atkinson:** Writing – review & editing, Validation, Supervision, Methodology. **Shan Huang:** Resources, Methodology. **Bruce E. Koel:** Conceptualization, Methodology. **Peter R. Jaffé:** Conceptualization, Writing – review & editing, Funding acquisition, Supervision.

Declaration of competing interest

The authors declare that they have no known competing financial interests or personal relationships that could have appeared to influence the work reported in this paper.

Acknowledgements

This work was supported by the National Institute of Environmental Health Sciences of the NIH (Grant Number R01ES032694). We also thank the High Meadows Environmental Institute at Princeton University for support through the Mary and Randall Hack '69 Graduate Award for Water and the Environment. The authors acknowledge the use of Princeton's Imaging and Analysis Center (IAC), which is partially supported by the Princeton Center for Complex Materials (PCCM), a National Science Foundation (NSF) Materials Research Science and Engineering Center (MRSEC; DMR-2011750).

Appendix A. Supplementary material

The Supplementary Material provides additional information supporting the geochemical, mineralogical, and microbial analyses presented in the main text. It includes detailed descriptions of Fe oxide characterization and experimental procedures (Text S1–S2), as well as supplementary methods and results for microbial community analysis (Text S3). Comparative data on Fe oxide morphology and crystallinity are provided in Figures S1–S2. Additional datasets include HCl-extractable Fe measurements from microbial incubations (Figures S3–S4), electron recovery efficiencies (Table S1), ammonium concentrations in *G. sulfurreducens* pure cultures (Figure S5), substrate concentrations in autoclaved controls (Figure S6), and redox and pH trends during microbial incubations (Figures S7–S8). Further supplemental information includes corrections for A6-driven ammonium removal in co-cultures (Figure S9), detailed XANES–LCF results for Fe K-edge spectra (Table S2), and microbial diversity and OTU abundance analyses (Table S3; Figures S10–S11). Supplementary material to this article can be found online at https://doi.org/10.1016/j.gca.2026.03.050.

Data availability

Data are available through Zenodo at: https://doi.org/10.5281/zenodo.17672259.

References

Amer, A., Kim, Y., 2023. Minimizing the lag phase of *Cupriavidus necator* growth under autotrophic, heterotrophic, and mixotrophic conditions. Appl. Environ. Microbiol. 89 (2), e02007–e2022.

Amstaetter, K., Borch, T., Larese-Casanova, P., Kappler, A., 2010. Redox transformation of arsenic by Fe(II)-activated goethite (α-FeOOH). Environ. Sci. Technol. 44 (1), 102–108.

Boland, D.D., Collins, R.N., Miller, C.J., Glover, C.J., Waite, T.D., 2014. Effect of solution and solid-phase conditions on the Fe(II)-accelerated transformation of ferrihydrite to lepidocrocite and goethite. Environ. Sci. Technol. 48 (10), 5477–5485.

Bond, D.R., Lovley, D.R., 2003. Electricity production by *Geobacter sulfurreducens* attached to electrodes. Appl. Environ. Microbiol. 69 (3), 1548–1555.

Bonneville, S., Behrends, T., Van Cappellen, P., 2009. Solubility and dissimilatory reduction kinetics of iron(III) oxyhydroxides: a linear free energy relationship. Geochim. Cosmochim. Acta 73 (18), 5273–5282.

Callister Jr., W.D., Rethwisch, D.G., 2020. *Materials science and engineering: An introduction*. John Wiley & Sons.

Chan, C.H., Levar, C.E., Zacharoff, L., Badalamenti, J.P., Bond, D.R., 2015. Scarless genome editing and stable inducible expression vectors for *Geobacter sulfurreducens*. Appl. Environ. Microbiol. 81 (20), 7178–7186.

Coppi, M.V., Leang, C., Sandler, S.J., Lovley, D.R., 2001. Development of a genetic system for *Geobacter sulfurreducens*. Appl. Environ. Microbiol. 67 (7), 3180–3187.

Cutting, R., Coker, V., Fellowes, J., Lloyd, J., Vaughan, D., 2009. Mineralogical and morphological constraints on the reduction of Fe(III) minerals by *Geobacter sulfurreducens*. Geochim. Cosmochim. Acta 73 (14), 4004–4022.

Esteve-Núñez, A., Rothermich, M., Sharma, M., Lovley, D., 2005. Growth of *Geobacter sulfurreducens* under nutrient-limiting conditions in continuous culture. Environ. Microbiol. 7 (5), 641–648.

Hansel, C.M., Benner, S.G., Fendorf, S., 2005. Competing Fe(II)-induced mineralization pathways of ferrihydrite. Environ. Sci. Technol. 39 (18), 7147–7153.
Hansel, C.M., Benner, S.G., Neiss, J., Dohnalkova, A., Kukkadapu, R.K., Fendorf, S., 2003. Secondary mineralization pathways induced by dissimilatory iron reduction of ferrihydrite under advective flow. Geochim. Cosmochim. Acta 67 (16), 2977–2992.
Howley, E., Ki, D., Krajmalnik-Brown, R., Torres, C.I., 2022. *Geobacter sulfurreducens*' unique metabolism results in cells with a high iron and lipid content. Microbiol. Spectr., 10 (6), e02593–02522.
Huang, S., Jaffé, P.R., 2015. Characterization of incubation experiments and development of an enrichment culture capable of ammonium oxidation under iron-reducing conditions. Biogeosciences 12 (3), 769–779.
Huang, S., Jaffé, P.R., 2018. Isolation and characterization of an ammonium-oxidizing iron reducer: *Acidimicrobiaceae* sp. A6. PLoS One 13 (4), e0194007.
Huang, S., Jaffé, P.R., 2019. Defluorination of perfluorooctanoic acid (PFOA) and perfluorooctane sulfonate (PFOS) by *Acidimicrobium* sp. strain A6. Environ. Sci. Technol. 53 (19), 11410–11419.
Huang, S., Pilloni, G., Key, T.A., Jaffé, P.R., 2024a. Defluorination of various perfluoro alkyl acids and selected PFOA and PFOS monomers by *Acidimicrobium* sp. strain A6 enrichment cultures. J. Hazard. Mater. 480, 136426.
Huang, S., Sima, M., Long, Y., Messenger, C., Jaffé, P.R., 2022. Anaerobic degradation of perfluorooctanoic acid (PFOA) in biosolids by *Acidimicrobium* sp. strain A6. J. Hazard. Mater. 424, 127699.
Huang, S., Smorada, C., Schaefer, C.E., Jaffé, P.R., 2024b. Stimulating *Acidimicrobium* sp. strain A6 in iron-rich, acidic sediments from AFFF-impacted sites for PFAS defluorination. Sci. Total Environ. 955, 176801.
Jaffé, P.R., Huang, S., Park, J., Ruiz-Urigüen, M., Shuai, W., Sima, M., 2024. Defluorination of PFAS by *Acidimicrobium* sp. strain A6 and potential applications for remediation. Methods Enzymol. Elsevier 287–320.
Latta, D.E., Bachman, J.E., Scherer, M.M., 2012. Fe electron transfer and atom exchange in goethite: influence of Al-substitution and anion sorption. Environ. Sci. Technol. 46 (19), 10614–10623.
Lentini, C.J., Wankel, S.D., Hansel, C.M., 2012. Enriched iron(III)-reducing bacterial communities are shaped by carbon substrate and iron oxide mineralogy. Front. Microbiol. 3, 404.
Li, X., Hou, L., Liu, M., Zheng, Y., Yin, G., Lin, X., Cheng, L., Li, Y., Hu, X., 2015. Evidence of nitrogen loss from anaerobic ammonium oxidation coupled with ferric iron reduction in an intertidal wetland. Environ. Sci. Technol. 49 (19), 11560–11568.
Lovley, D.R., Phillips, E.J., 1988. Novel mode of microbial energy metabolism: organic carbon oxidation coupled to dissimilatory reduction of iron or manganese. Appl. Environ. Microbiol. 54 (6), 1472–1480.
Marsili, E., Rollefson, J.B., Baron, D.B., Hozalski, R.M., Bond, D.R., 2008. Microbial biofilm voltammetry: direct electrochemical characterization of catalytic electrode-attached biofilms. Appl. Environ. Microbiol. 74 (23), 7329–7337.
Nakamura, R., Kai, F., Okamoto, A., Hashimoto, K., 2013. Mechanisms of long-distance extracellular electron transfer of metal-reducing bacteria mediated by nanocolloidal semiconductive iron oxides. J. Mater. Chem. A 1 (16), 5148–5157.
Nevin, K.P., Lovley, D.R., 2002. Mechanisms for accessing insoluble Fe(III) oxide during dissimilatory Fe(III) reduction by *Geothrix fermentans*. Appl. Environ. Microbiol. 68 (5), 2294–2299.
Notini, L., Latta, D.E., Neumann, A., Pearce, C.I., Sassi, M., N'Diaye, A.T., Rosso, K.M., Scherer, M.M., 2018. The role of defects in Fe(II)–goethite electron transfer. Environ. Sci. Technol. 52 (5), 2751–2759.
Notini, L., Byrne, J.M., Tomaszewski, E.J., Latta, D.E., Zhou, Z., Scherer, M.M., Kappler, A., 2019. Mineral defects enhance bioavailability of goethite toward microbial Fe(III) reduction. Environ. Sci. Technol. 53 (15), 8883–8891.
O'loughlin, E.J., Boyanov, M.I., Gorski, C.A., Scherer, M.M., Kemner, K.M., 2021. Effects of Fe(III) oxide mineralogy and phosphate on Fe(II) secondary mineral formation during microbial iron reduction. Minerals 11 (2), 149.
Park, J., Huang, S., Koel, B.E., Jaffé, P.R., 2023. Enhanced feammox activity and perfluorooctanoic acid (PFOA) degradation by *Acidimicrobium* sp. strain A6 using PAA-coated ferrihydrite as an electron acceptor. J. Hazard. Mater. 459, 132039.
Ravel, B., Newville, M., 2005. ATHENA, ARTEMIS, HEPHAESTUS: data analysis for X-ray absorption spectroscopy using IFEFFIT. Synchrotron Radiation 12 (4), 537–541.
Roden, E.E., Urrutia, M.M., 2002. Influence of biogenic Fe(II) on bacterial crystalline Fe (III) oxide reduction. Geomicrobiol J. 19 (2), 209–251.
Ruiz-Urigüen, M., Shuai, W., Huang, S., Jaffé, P.R., 2022. Biodegradation of PFOA in microbial electrolysis cells by *Acidimicrobiaceae* sp. strain A6. Chemosphere 292, 133506.
Sawayama, S., 2006. Possibility of anoxic ferric ammonium oxidation. J. Biosci. Bioeng. 101 (1), 70–72.
Schwertmann, U., Cornell, R.M., 2008. Iron oxides in the laboratory: preparation and characterization. John Wiley & Sons.
Sheng, A., Liu, J., Li, X., Qafoku, O., Collins, R.N., Jones, A.M., Pearce, C.I., Wang, C., Ni, J., Lu, A., 2020. Labile Fe(III) from sorbed Fe(II) oxidation is the key intermediate in Fe(II)-catalyzed ferrihydrite transformation. Geochim. Cosmochim. Acta 272, 105–120.
Shuai, W., Jaffé, P.R., 2019. Anaerobic ammonium oxidation coupled to iron reduction in constructed wetland mesocosms. Sci. Total Environ. 648, 984–992.
Sima, M.W., Huang, S., Jaffé, P.R., 2023. Modeling the kinetics of perfluorooctanoic and perfluorooctane sulfonic acid biodegradation by *Acidimicrobium* sp. strain A6 during the feammox process. J. Hazard. Mater. 448, 130903.
Stookey, L.L., 1970. Ferrozine—a new spectrophotometric reagent for iron. Anal. Chem. 42 (7), 779–781.
Straub, K.L., Buchholz-Cleven, B., 2001. *Geobacter bremensis* sp. nov. and *Geobacter pelophilus* sp. nov., two dissimilatory ferric-iron-reducing bacteria. Int. J. Syst. Evol. Microbiol. 51 (5), 1805–1808.
Stults, J.R., Snoeyenbos-West, O., Methe, B., Lovley, D.R., Chandler, D.P., 2001. Application of the 5′ fluorogenic exonuclease assay (TaqMan) for quantitative ribosomal DNA and rRNA analysis in sediments. Appl. Environ. Microbiol. 67 (6), 2781–2789.
Viollier, E., Inglett, P., Hunter, K., Roychoudhury, A., Van Cappellen, P., 2000. The ferrozine method revisited: Fe(II)/Fe(III) determination in natural waters. Appl. Geochem. 15 (6), 785–790.
Wang, T., Zhu, G., Kuang, B., Jia, J., Liu, C., Cai, G., Li, C., 2021. Novel insights into the anaerobic digestion of propionate via *Syntrophobacter fumaroxidans* and *Geobacter sulfurreducens*: process and mechanism. Water Res. 200, 117270.
Xu, Z., Masuda, Y., Itoh, H., Ushijima, N., Shiratori, Y., Senoo, K., 2019. *Geomonas oryzae* gen. nov., sp. nov., *Geomonas edaphica* sp. nov., *Geomonas ferrireducens* sp. nov., *Geomonas terrae* sp. nov., four ferric-reducing bacteria isolated from paddy soil, and reclassification of three species of the genus *Geobacter* as members of the genus *Geomonas* gen. nov. Front. Microbiol. 10, 2201.
Zachara, J.M., Fredrickson, J.K., Li, S.-M., Kennedy, D.W., Smith, S.C., Gassman, P.L., 1998. Bacterial reduction of crystalline Fe^{3+} oxides in single phase suspensions and subsurface materials. Am. Mineral. 83 (11–12 Part 2), 1426–1443.
Zachara, J.M., Kukkadapu, R.K., Fredrickson, J.K., Gorby, Y.A., Smith, S.C., 2002. Biomineralization of poorly crystalline Fe(III) oxides by dissimilatory metal reducing bacteria (DMRB). Geomicrobiol J. 19 (2), 179–207.